Modeling of Imperfect Mixing and Its Effects on Polymer Properties

Simon X. Zhang and W. Harmon Ray
Dept. of Chemical Engineering, University of Wisconsin-Madison, Madison, WI 53706

A compartmental model is used to study imperfect mixing and its effects on polymer properties. Examples of imperfect feed mixing caused by a rapidly decomposing initiator are shown for styrene polymerization, high-pressure ethylene polymerization, and vinyl acetate/methyl methacrylate solution copolymerization. Continuation analysis indicates mixing can change reactor steady states and stability. A composite approach is proposed to construct full molecular weight distribution (MWD) under imperfect mixing. In linear polymerization imperfect mixing broadens MWD; however, in nonlinear polymerization mixing can cause either broader or narrower MWD. By changing the dominant chain-termination mechanism to chain transfer, the influence of imperfect mixing on the MWD can be reduced. Depending on reactivity ratio and monomer composition, mixing also affects copolymer composition and chain sequence length.

Introduction

In order for bimolecular reactions to occur, reactants have to be brought into contact with each other. When the rates of reaction and mixing are similar, a strong interaction exists between these two processes. This interaction is especially important in polymerization reactors because not only reactor productivity, but also polymer properties can be significantly affected by mixing.

Imperfect mixing generally refers to the nonhomogeneity of species concentration inside the reactor at both macroscopic and microscopic levels. Macromixing deals with mixing on the reactor scale, such as mixing caused by a velocity field; while micromixing is concerned with mixing on the molecular scale because a macroscopically well-mixed fluid may not be well-mixed microscopically.

Mixing effects have been reported in many polymerization systems, such as continuous styrene polymerization with a fast decomposing initiator (Sahm, 1978; Villermaux, 1991), styrene solution polymerization at high conversions (Harada et al., 1968), styrene suspension polymerization under ultrasonic radiation (Hatate et al., 1981), and vinyl acetate suspension polymerization (Baade et al., 1982).

Mixing affects monomer conversion, initiator consumption (van der Molen and Keonen, 1981; Marini and Georgakis, 1984a), copolymer composition distribution (CCD) (Atiqullah and Nauman, 1990; Mecklenburgh, 1970; O'Driscoll and Knorr, 1969), and the molecular-weight distribution (MWD) (Tadmor and Biesenberger, 1966; Marini and Georgakis, 1984b; Tosun, 1992). The mean values of CCD and MWD are less affected than the breadth of the distributions, which often increases with poorer mixing.

Because polymer properties are determined by many kinetic mechanisms, detailed kinetics are needed to understand the impacts of mixing on polymer properties. However, the articles discussing mixing effects in polymerization reactors only consider simplified kinetics or some specific systems. Little attention has been paid to understand the interaction between mixing and kinetics and the impact of mixing on polymer properties. This article intends to fill this gap, and its objective is a better fundamental understanding of the mixing effects on polymer properties.

In this article, a realistic compartmental mixing model is used to study imperfect mixing caused by fast decomposing initiators. Detailed polymerization kinetics is employed to understand the effects of mixing on polymer properties. Three polymerization systems are studied because of their industrial importance and distinct kinetics: styrene solution polymerization, which is a typical linear homopolymerization; high-pressure ethylene polymerization, which has significant branching reactions; and vinyl acetate/methyl methacrylate copolymerization, which has very different monomer reactiv-

Correspondence concerning this article should be addressed to W. H. Ray.
Present address of S. X. Zhang: Exxon Chemical Company, 5200 Bayway Drive, Baytown, TX 77520.

ity ratios. The results suggest that imperfect mixing has a different qualitative effect on the polymer properties, depending upon the kinetics involved.

Review of Imperfect Mixing Models

Many mixing models have been proposed in the literature, all of which consider the nonuniformity of species concentration inside the reactor. They can be loosely classified into three categories: *fluid-flow models*, *fluid-particle models*, and *fluid-mechanics models*. As suggested by Smit (1992), any model that explains *slowness* of mixing can describe experimentally determined variables, such as initiator consumption. Hence, another empirical or semiempirical mixing model does not represent a major contribution to the fundamental understanding of mixing in polymerization reactors.

Fluid-flow models

Fluid-flow models divide the reactor into several zones with well-defined macro- and micromixing characteristics and are simple but realistic mixing models. They can be further divided into compartmental and environmental models.

Compartmental models construct a flow sheet by connecting different reaction zones that are usually perfectly mixed continuous stirred-tank reactors (CSTRs). They mainly describe macromixing patterns inside the reactor when material transport between different zones is only by convection. However, they can also represent some degree of micromixing if diffusion is allowed between different zones (Villermaux, 1989a). Compartmental models have been used to study imperfect mixing in continuous LDPE autoclave (Marini and Georgakis, 1984a; Chan et al., 1993) and a semibatch reactor (Tosun, 1992). They have also been used to study the influence of mixing on reactor stability (Zacca et al., 1995) and interaction of mixing and gelation (Kalbfleisch and Teymour, 1995).

Environment models (Weinstein and Adler, 1967; Villermaux and Zoulalian, 1969; Mehta and Tarbell, 1983) represent imperfect mixing by a combination of environments, each in an extreme state of either perfect mixing or complete segregation. One or more free parameters control the amount of fluid entering each environment. If the flow characteristics remain the same, the parameters obtained from one kinetic scheme can be applied to another kinetic scheme.

Fluid-particle models

Fluid-particle models assume the reactor fluid consists of many droplets that interact in pairs by either diffusion or coalescence and redispersion. The resulting models are population balances over the droplet properties. Based on interaction mechanisms, they can be further divided into coalescence–redispersion (CRD) models, interaction by exchange with a mean environment (IEM) models, and composite models.

In CRD models, two fluid particles coalescence, completely mix their contents, and immediately break up into two particles. By varying the coalescence and breakage rate, the mixing conditions change from complete segregation to perfect mixing. Representative examples include the one by Curl (1963) for single CSTR and one by Kattan and Adler (1972) for arbitrary residence-time distribution. Because CRD models are difficult to solve for complex reactions, Monte Carlo simulations have also been applied (Spielman and Levenspiel, 1964; Hatate et al., 1981).

IEM model assumes that interaction between different fluid particles can be represented by a mass-transfer process with an environment having the mean concentration of all the particles (Villermaux, 1991). By varying the ratio of reactor residence time to micromixing time, the reactor changes from perfect mixing to complete segregation. It has also been applied to both macro- and micromixing (Fox and Villermaux, 1990).

Composite models combine environment and fluid-particle models, where intermediate mixing is allowed within each environment. They are proposed to correct drawbacks of the original approaches, but introduce some additional complexity (Goto and Matsubara, 1975; Ritchie and Tobgy, 1978; Call and Kadlec, 1989).

Fluid-mechanics models

Fluid-mechanics models try to describe the mixing phenomena from first principles. They have a more sound theoretical basis, but have difficulty handling complex geometry and reaction kinetics. Some fluid-mechanics models are based on ultimate microturbulence and molecular diffusion of the fluid element (Nauman, 1975; Baldyga and Bourne, 1984; Fields and Ottino, 1987).

The most recent development in modeling imperfect mixing is computational fluid dynamics (CFD) that solves the governing equations of the flow and yields a complete flow field. CFD has recently been applied to model imperfect mixing in high-pressure ethylene polymerization in autoclave and tubular reactors (Torvik et al., 1995; Tsai and Fox, 1995; Read et al., 1996). Although CFD is a powerful tool in handling mixing in a complex geometry, it still suffers from very long computation times and difficulties in handling micromixing effectively.

Free-radical Polymerization Kinetics

A general kinetic model for free-radical polymerization is developed based on the kinetic model developed for addition polymerization (Arriola, 1989). It predicts polymer chain-length distributions, copolymer composition, and chain sequence length. Table 1 summarizes the major kinetics steps. In the table, $D_{n,b}$ refers to dead polymer with chain length n and trifunctional branching points b; $P_{i,n,b}$ represents the live polymer with chain length n, trifunctional branching points b and end group of type i.

The model is developed on the basis of the following assumptions:

- Long chain approximation.
- Quasi-steady-state approximation (QSSA) for live radicals and instantaneous properties.
- Reactivity of a live polymer chain depends only on the end-group type.
- Transfer to polymer assumes that bulk copolymer composition is homogeneous with respect to the chain-length distribution.

Table 1. Free-Radical Polymerization Kinetics

Initiation	
Peroxide or azo-compound	$I \xrightarrow{fk_d} 2R\cdot$
decomposition	$R\cdot + M \xrightarrow{fast} P_{1,0}$
Special initiation	$C + M \xrightarrow{gk_i} P_{1,0}$
Propagation	
Forward and reverse	$P_{n,b} + M \xleftrightarrow{k_p} P_{n+1,b}$
Termination	
By coupling	$P_{n,b} + P_{m,c} \xrightarrow{k_{tc}} D_{n+m,b+c}$
By disproportionation	$P_{n,b} + P_{m,c} \xrightarrow{k_{td}} D_{n,b} + D_{m,c}$
By inhibition	$P_{n,b} + X \xrightarrow{k_{tx}} D_{n,b}$
Spontaneous	$P_{n,b} \xrightarrow{k_{tsp}} D_{n,b}$
Chain transfer	
To monomer	$P_{n,b} + M \xrightarrow{k_{trm}} D_{n,b} + M\cdot$
To solvent	$P_{n,b} + S \xrightarrow{k_{trs}} D_{n,b} + S\cdot$
To transfer agent	$P_{n,b} + T \xrightarrow{k_{tra}} D_{n,b} + A\cdot$
Spontaneous	$P_{n,b} \xrightarrow{k_{trsp}} D_{n,b} + H\cdot$
Reinitiation	$M\cdot, S\cdot, A\cdot, H\cdot + M \xrightarrow{fast} P_{1,0}$
Backbiting	$P_{n,b} \xrightarrow{k_b} Q_{n,b}$
Scission after backbiting	$P_{n,b} \xrightarrow{p_b k_{\beta 1}} D_{n-q,b} + P_{q,0}$
Transfer to polymer	$P_{n,b} + D_{m,c} \xrightarrow{mk_{trp}} D_{n,b} + P_{m,c+1}$
Scission after transfer to polymer	$P_{n,b+1} \xrightarrow{p_{trp} k_{\beta 2}} D_{u,v} + P_{n-u,b-v}$
Terminal double bond	$P_{n,b} + D_{m,c} \xrightarrow{dk_{TDB}} D_{n+m,b+c+1}$

Table 2. Apparent Rate Constants of Free-radical Copolymerization

$$k_p = \sum_{i=1}^{N}\sum_{j=1}^{N} k_{p_{ij}} P^i F_{M_j} \qquad k_{prv} = \sum_{i=1}^{N} k_{prv_{ii}} P^i \epsilon_{ii}$$

$$k_{tc} = \sum_{i=1}^{N}\sum_{j=1}^{N} k_{tc_{ij}} P^i P^j \qquad k_{td} = \sum_{i=1}^{N}\sum_{j=1}^{N} k_{td_{ij}} P^i P^j$$

$$k_{tx} = \sum_{i=1}^{N} k_{tx_i} P^i \qquad k_{tsp} = \sum_{i=1}^{N} k_{tsp_i} P^i$$

$$k_{trm} = \sum_{i=1}^{N}\sum_{j=1}^{N} k_{trm_{ij}} P^i F_{M_j} \qquad k_{trs} = \sum_{i=1}^{N}\sum_{j=1}^{N} k_{trs_i} P^i$$

$$k_{tra} = \sum_{i=1}^{N} k_{tra_i} P^i \qquad k_{trsp} = \sum_{i=1}^{N} k_{trsp_i} P^i$$

$$k_{trp} = \sum_{i=1}^{N}\sum_{j=1}^{N} k_{trp_{ij}} P^i F_{P_j} \qquad k_b = \sum_{i=1}^{N}\sum_{j=1}^{N} k_{b_{ij}} P^i \mathrm{Inst} F_{P_j}$$

$$k_{\beta 1} = \sum_{i=1}^{N} k_{\beta 1_i} \mathrm{Inst} F_{P_i} \qquad k_{\beta 2} = \sum_{i=1}^{N} k_{\beta 2_i} \mathrm{Inst} F_{P_i}$$

$$k_{TDB} = \sum_{i=1}^{N}\sum_{j=1}^{N} k_{TDB_{ij}} P^i F_{d_j}$$

Kinetic rate constants

The reaction rate constants are calculated from a generalized Arrhenius form, with the inclusion of activation volume V_a and centering factor C_c

$$k = k_0 \exp\left(- \frac{E_a + PV_a}{RT} + C_c \right). \tag{1}$$

The copolymerization systems are modeled with a pseudo-homopolymerization approach based on the instantaneous property method (Hamielec and MacGregor, 1983; Kuo et al., 1984). A set of apparent rate constants is calculated from the instantaneous monomer and copolymer properties. Homopolymerization can be directly applied except for the copolymer properties. A complete list of apparent rate constants is given in Table 2.

Gel effect is modeled by multiplying the propagation and termination rate constants by gel-effect factors. The gel-effect correlations used are the same as those used by Kalfas and Ray (1993).

Polymer moment equations

The method of moments is used to calculate polymer MWD (Ray, 1972). The live and total polymer number chain-length distribution (NCLD) moments are defined as

Live polymer moments:

$$\mu_{i,j} = \sum_{n=1}^{\infty}\sum_{b=0}^{\infty} n^i b^j P_{n,b} \tag{2}$$

Bulk polymer moments:

$$\lambda_{i,j} = \sum_{n=1}^{\infty}\sum_{b=0}^{\infty} n^i b^j (P_{n,b} + D_{n,b}). \tag{3}$$

Applying the moment definition (Eqs. 2 and 3) to the population balance of polymeric species yields the moment balance equations. Complete moment balance equations for a single CSTR up to the third moments are given in the Appendix. Bulk polymer properties can be calculated from the bulk polymer moments.

- Degree of polymerization: $DP_n = \lambda_{1,0}/\lambda_{0,0}$
- Polydispersity: $Z_p = (\lambda_{2,0}\lambda_{0,0})/\lambda_{1,0}^2$
- Branching degree: $B_n = \lambda_{0,1}/\lambda_{0,0}$
- Branching dispersity: $Z_b = (\lambda_{1,1}\lambda_{0,0})/(\lambda_{1,0}\lambda_{0,1})$

Instantaneous copolymer properties

Radical Composition. Under the long-chain approximation, the instantaneous radical composition P^i is determined only by the propagation reaction. The rate of change of live polymer chain of j type is

$$R_{P_j} = \sum_{i=1}^{N} k_{p_{ij}} P^i C_{M_j} - \sum_{i=1}^{N} k_{p_{ji}} P^j C_{M_i}. \tag{4}$$

Under the QSSA, rates of change of live polymer are set zero: $R_{P_j} = 0$, $j = 1, \ldots, N$. Preceding N linear equations can

then be solved for the instantaneous radical composition.

Copolymer Composition. The instantaneous copolymer composition is the instantaneous monomer mole fractions incorporated into the polymer:

$$\text{Inst}F_{P_j} = \frac{R_{M_j}}{\sum_{i=1}^{N} R_{M_i}}, \tag{5}$$

where the monomer consumption rates are

$$R_{M_j} = \left\{ \sum_{i=1}^{N} k_{p_{ij}} P_n^i \right\} C_{M_j}. \tag{6}$$

Chain Sequence Length. The probability of forming n sequential units of monomer j in the growing polymer chain is given by

$$P_{L_j^n} = p_{jj}^{n-1}(1 - p_{jj}) \tag{7}$$

$$p_{jj} = \frac{k_{p_{jj}} C_{M_j}}{\sum_{i=1}^{N} k_{p_{ji}} C_{M_i}} = \frac{F_{M_i}}{\sum_{i=1}^{N} \frac{F_{M_i}}{r_{ji}}}. \tag{8}$$

The instantaneous average chain sequence length for monomer j is

$$\text{Inst}SL_j = \sum_{n=1}^{\infty} n p_{jj}^{n-1}(1 - p_{jj}) \tag{9}$$

$$= \frac{1}{1 - p_{jj}}. \tag{10}$$

Cumulative properties

Unreacted Monomer Composition. The balance equation for unreacted monomer i in a CSTR is

$$\frac{d(VC_m F_{m_i})}{dt} = Q^{\text{in}} C_m^{\text{in}} F_{m_i}^{\text{in}} - Q^{\text{out}} C_m F_{m_i} - VR_{\lambda_{10}} \text{Inst}F_{m_i}. \tag{11}$$

From the total unreacted monomer balance around the reactor, we have

$$\frac{d(VC_m)}{dt} = Q^{\text{in}} C_m^{\text{in}} - Q^{\text{out}} C_m - VR_{\lambda_{10}}. \tag{12}$$

Substitution of Eq. 12 into the individual monomer balance equation, Eq. 11, gives

$$VC_m \frac{dF_{m_i}}{dt} = Q^{\text{in}} C_m^{\text{in}} \left(F_{m_i}^{\text{in}} - F_{m_i} \right) + VR_{\lambda_{10}} (F_{m_i} - \text{Inst}F_{m_i}). \tag{13}$$

Copolymer Composition. Similar to the derivation of F_{M_i}, copolymer composition in a CSTR is given by

$$VC_p \frac{dF_{p_i}}{dt} = Q^{\text{in}} C_p^{\text{in}} \left(F_{p_i}^{\text{in}} - F_{p_i} \right) - VR_{\lambda_{10}} (F_{p_i} - \text{Inst}F_{p_i}). \tag{14}$$

Chain Sequence Length. Chain sequence length in a CSTR can be obtained by integrating the corresponding instantaneous properties over time (Arriola, 1989):

$$\frac{dSL_j}{dt} = \Omega_p SL_j \frac{F_{P_j}^{\text{in}}}{F_{P_j}} \left(1 - \frac{SL_j}{SL_j^{\text{in}}} \right) + \Psi_p SL_j \frac{\text{Inst}F_{P_j}}{F_{P_j}} R_{\lambda_{10}} \left(1 - \frac{SL_j}{\text{Inst}SL_j} \right), \tag{15}$$

where

$$\Psi_p = \frac{MW_p}{1{,}000 \rho (1 - W_s) X_p} \tag{16}$$

$$\Omega_p = \frac{Q^{\text{in}} C_p^{\text{in}}}{VC_p}. \tag{17}$$

Compartmental Mixing Model

In many polymerization reactors, imperfect feed mixing happens when initiator lifetime is comparable to polymerization time, which is usually related to the reactor residence time. Under these conditions, it is difficult to mix the feed plume well before it is consumed. The initiator concentration is not uniform throughout the reactor, which in turn affects the reactor operation and polymer properties.

A compartmental model is employed to model this imperfect feed mixing; the model consists of two small mixing zones followed by a main reaction zone with recycle to represent the jet inflow. In the Figure 1, f_r is the total fraction of recycle volume to the two small zones; f_1 and f_2 are the fractions of the total recycle stream going to zone 1 and zone 2, respectively. The ratio of f_1 to f_2 is assumed to be the same as the volume ratio of zone 1 to zone 2 to reflect the volume difference between the two small mixing zones. This mixing model is similar to the one proposed by Marini and Georgakis (1984a) and the partially segregated feed model of Villermaux (1989b). The mixing parameters have been

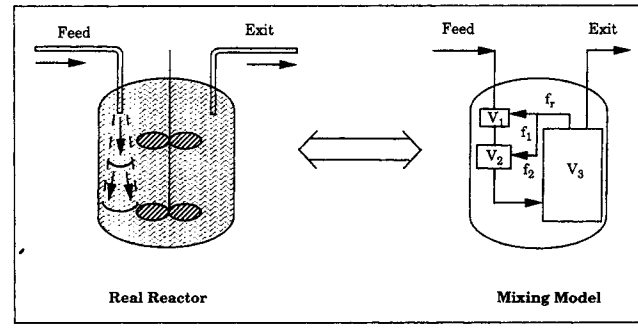

Figure 1. Compartmental mixing model.

Model for an imperfectly mixed reactor with feed entering as a plume. The model consists of a main reaction zone with two small mixing zones in series to represent the jet inflow.

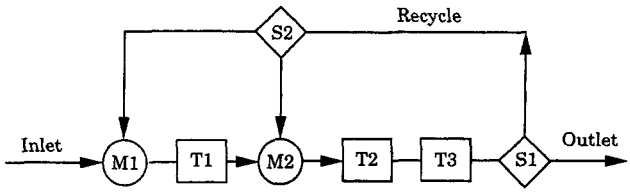

Figure 2. Flowsheet of a compartmental mixing model.

The flow sheet consists of three perfectly mixed tank reactors, two stream mixers, and two stream splitters.

successfully estimated from system responses to different disturbances (Zhang, 1996).

A distinctive feature of the present mixing model is the modular structure as shown in Figure 2. The whole flowsheet consists of three basic units: well-mixed tank reactor, stream mixer, and splitter. These basic units are independent modules with compatible stream structure so that they can be connected into different flowsheets.

Homogeneous tank reactor

Balance equations for the well-mixed tank reactor include:

- Material balances for monomer, polymer, and other species.
- Moment balances for polymer MWD.
- An energy balance for reactor temperature.

Only monomer, polymer, and solvent are considered to have significant volume. Other species, such as initiator, modifier, and inhibitor, exist only in tracer amounts and have negligible volume contribution.

Component densities and heat capacities are polynomial functions of reactor temperature and pressure. The reacting mixture properties are calculated from individual-component physical properties assuming volume additivity.

Material Balance. A total material balance around the well-mixed reactor yields

$$\frac{d(V\rho)}{dt} = Q^{\text{in}}\rho^{\text{in}} - Q\rho \tag{18}$$

The balances for other nonpolymer species in the tank are:

- Initiator

$$\frac{dW_I}{dt} = \frac{Q^{\text{in}}\rho^{\text{in}}}{V\rho}(W_I^{\text{in}} - W_I) - fk_dW_I \tag{19}$$

- Solvent

$$\frac{dW_S}{dt} \simeq \frac{Q^{\text{in}}\rho^{\text{in}}}{V\rho}(W_S^{\text{in}} - W_S) \tag{20}$$

- Inhibitor

$$\frac{dW_X}{dt} = \frac{Q^{\text{in}}\rho^{\text{in}}}{V\rho}(W_X^{\text{in}} - W_X) - k_{tx}W_X\mu_{0,0} \tag{21}$$

- Chain transfer agents

$$\frac{dW_A}{dt} = \frac{Q^{\text{in}}\rho^{\text{in}}}{V\rho}(W_A^{\text{in}} - W_A) - k_{tra}W_A\mu_{0,0}. \tag{22}$$

Energy Balance. The total energy balance around the well-mixed tank reactor is

$$\frac{d(V\rho e)}{dt} + c\frac{dT}{dt} = Q^{\text{in}}\rho^{\text{in}}e^{\text{in}} - Q\rho e + Ve_{rxn} + E_{\text{input}} - U_jA_j(T - T_j) \tag{23}$$

$$e = \int_{T_{\text{ref}}}^{T} c_p\,dT, \tag{24}$$

where c is the reactor-wall heat capacity, e is the enthalpy of the reaction mixture, and U_j is the overall heat transfer coefficient for the jacket.

Stream mixer and splitter

The stream mixer combines two incoming streams and has only one state, temperature. The outlet stream is calculated from inlets assuming simple mixing rules and averaging polymer moments.

The splitter divides one inlet stream into two outlet streams that have the same temperature, pressure, and composition as the inlet. The splitter also has no volume and dynamics and has only one design variable, the volume fractions of the inlet directed to the side outlet.

Numerical solution

The material, energy, and polymer moment balances, as well as the equations resulting from recycle streams are represented by a set of differential and algebraic equations. These equations, which can be written as

$$f(x, \dot{x}, \theta, t) = 0, \tag{25}$$

implicitly describe the relationship between states x, time derivative of the states $\dot{x}$, model parameters θ, and time t. The simulation, parameter estimation, and continuation analysis have been carried out under the framework of the POLYRED package developed in our group. A detailed discussion of POLYRED capabilities is presented elsewhere (Hyanek et al., 1995; Zacca et al., 1995; Ochs et al., 1996).

Continuous Styrene Polymerization

In polymerization reactions with fast decomposing initiators, mixing influences the initiator concentrations inside the reactor, which in turn affects the polymer MWD through the chain growth process. Sahm (1978) studied styrene solution polymerization with fast decomposing initiators. The experiments were carried out in a standard 670-cm^3 baffled reactor equipped with 6-blade turbine. Cyclohexane was used as solvent to keep the reaction medium at a constant low viscosity. Mixing effects were found when using fast decomposing initiators, such as PERKADOX 16 (bis-4-*t*-butylcyclohexyl per-

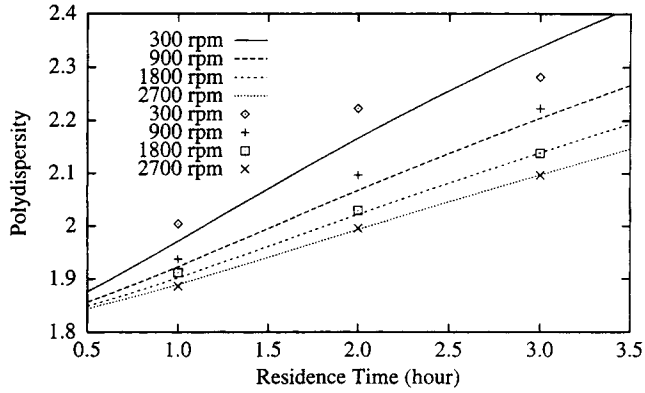

Figure 3. Effects of mixing on polydispersity.

Styrene solution polymerization in an imperfectly mixed CSTR. The mixing model prediction is compared with the experimental results from Villermaux (1991). The reactor is operated isothermally at 75°C with cyclohexane as solvent.

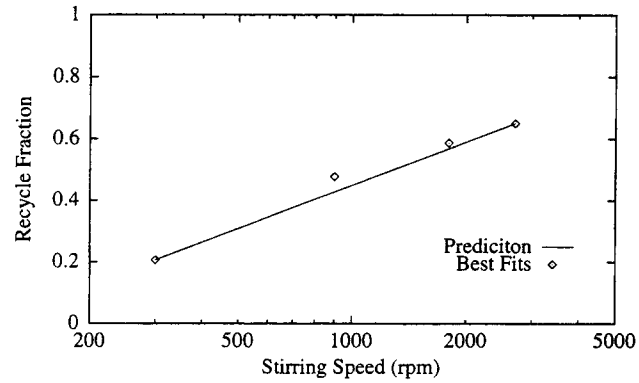

Figure 4. Prediction of mixing parameters.

The recycle fraction f_r is predicted from the semilog correlation using the f_r values estimated at other mixing conditions.

oxydicarbinate). Polydispersity (M_w/M_n) increases with increasing residence time and decreasing stirring speed suggest that the MWD depends on the mixing conditions.

With the compartmental mixing model, polydispersities at 900 and 1,800 rpm are predicted using mixing parameters estimated at 300 and 3,600 rpm. The experimental results and the model predictions are shown in Figure 3. The kinetic parameters used in simulation are obtained from the open literature (Blavier and Villermaux, 1984) and are listed in Table 3. The only adjustable mixing parameter is the recycle fraction from the main reaction zone to the two small inlet mixing zones f_r. The values of f_r at 300 and 3,600 rpm were estimated using the parameter estimation driver (PED) of the POLYRED package. Since the local mixing energy dissipation rate ϵ is proportional to N^2D^3, where N and D are the impeller speed and diameter, f_r is correlated linearly to the logarithm of the stirring speed N as shown in Figure 4. The semilog correlation results, and the best fits from the experiments at 900 and 1,800 rpm are very close.

The differences between the model prediction and the experiments at low stirring speed is mainly caused by keeping all the other mixing parameters independent of stirring speed. Apparently, the mixing zone size may also change if the stirring speed varies over a wide range. Better fit can be achieved by using more adjustable parameters. However, this will increase the freedom of estimation and reduce the prediction power of the model. Furthermore, the normal precision in polydispersity measured by gel permeation chromatography (GPC) suggests that the difference between the prediction and experiments is close to experimental error. Taking these factors into consideration, the agreement between model prediction and experiments is quite reasonable.

Table 3. Kinetic Rate Constants of Styrene Polymerization*

Reaction	Rate Constants at 75°C
Initiation k_d (Perkadox 16)	1.23×10^{-3} s^{-1} $f = 0.5$
Propagation k_p	2.40×10^{2} L·mol^{-1}·s^{-1}
Combination k_{tc}	2.00×10^{7} L·mol^{-1}·s^{-1}
Disproportionation k_{td}	1.10×10^{7} L·mol^{-1}·s^{-1}
Transfer to monomer k_{trm}	1.52×10^{-1} L·mol^{-1}·s^{-1}

*Parameters are from Blavier and Villermaux (1984). k_{tc} is modified to match the polydispersity under the perfect mixing condition.

Imperfect Mixing in Low-density Polyethylene Autoclaves

In a typical low-density polyethylene (LDPE) autoclave reactor, the initiator half-life time is only several seconds; while reactor residence time is usually 30 to 60 s. Under these conditions, the initiator concentration is not uniform throughout the reactor.

Figure 5 shows the flow sheet and reaction conditions of an imperfectly mixed LDPE autoclave. The kinetic parameters used for the simulation are obtained from the available literature (Chen et al., 1976; Goto et al., 1981) and are listed in Table 4. The three reaction zones are assumed to be adiabatic CSTRs under constant pressure, typical of the real industrial autoclaves. The total recycle fraction (f_r) is 0.86, corresponding to a recycle ratio of 6.14, to represent the high stirring speeds and high mixing energy inputs commonly found in commercial operations. The feed conditions are the same for the well-mixed and imperfectly mixed reactors in order to show only the mixing effects.

Figure 6 shows the steady-state outlet temperature as a function of inlet initiator concentration. The reactor shows multiple steady states under the perfect and imperfect mixing. The lower steady states correspond to a reactor extinction; the upper steady states represent the normal operation conditions. For adiabatic reactors, monomer conversion is directly proportional to temperature rise. At the same inlet ini-

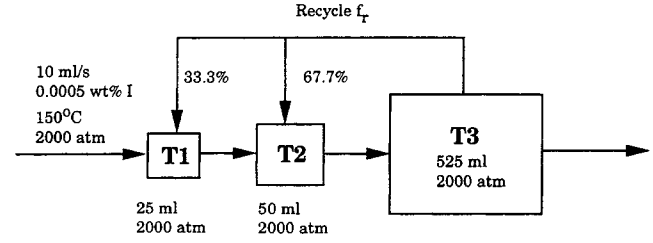

Figure 5. Flow sheet of an imperfect mixed LDPE autoclave reactor.

Table 4. Kinetic Rate Constants of High-pressure Ethylene Polymerization

Reaction	k_0 (L/mol·s)	E_a (cal/mol)	V_a* (cal/atm·mol)
Initiation k_d (DTBP)	1.81×10^{16}	38,400	0.0605
Propagation k_p	1.14×10^{7}	7,091	−0.477
Termination k_{tc}	3.00×10^{9}	2,400	0.3147
Transfer to polymer k_{trp}	1.11×10^{6}	9,000	0.1065
Transfer to solvent k_{trs}	6.44×10^{6}	9,391	−0.4722
Transfer to monomer k_{trm}	2.92×10^{6}	11,041	−0.484
Backbiting k_b	2.95×10^{7}	9,016	−0.5690
β-scission k_β	1.04×10^{12}	20,000	−0.465

*V_a can be converted to cm^3 using conversion factor of 41.293.

tiator concentration, a perfectly mixed reactor has a higher outlet (zone 3) temperature and monomer conversion. Thus improving initiator mixing can improve reactor productivity. However, if temperature is above 300°C, ethylene decomposing reactions become important and lead to a reactor runaway (Zhang et al., 1996).

Steady-state number (DP_n) and weight (DP_w) average chain length as a function of the inlet initiator concentration are shown in Figures 7 and 8. For both perfect and imperfect mixing, DP_n decreases with increasing initiator feed, while DP_w increases. Notice that in a perfectly mixed reactor DP_n is smaller while DP_w is larger than a corresponding imperfectly mixed one, resulting in a higher polydispersity.

Vinyl Acetate/MMA Copolymerization

To study the interaction between branching and mixing, the LDPE mixing model has been applied to solution copolymerization of vinyl acetate (VAc) and methyl methacrylate (MMA). The reactor is operated isothermally at 65°C with the mixing flow sheet and reaction conditions shown in Figure 9. Relatively long residence time (8 h) is chosen to show the more severe mixing cases. The initiator used is benzoyl phenylaceteyl peroxide (BPPO), an initiator with a relatively rapid rate of decomposition. The kinetic parameters are listed

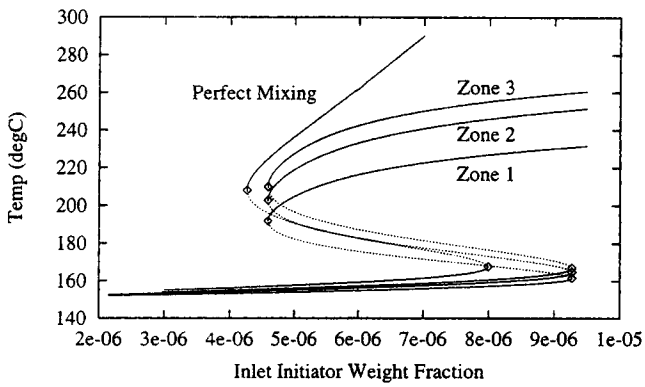

Figure 6. Continuation diagram of mixing-zone temperatures.

The steady-state temperatures in different mixing zones are shown as a function of the inlet initiator concentration.

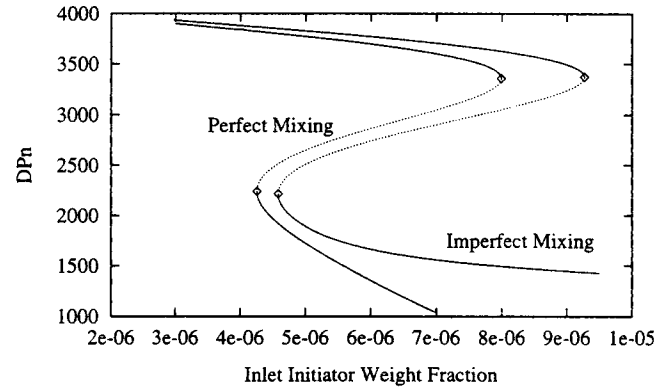

Figure 7. Continuation diagram of number average chain length.

Steady-state number average chain length (DP_n) is shown as a function of the inlet initiator concentration under both perfect and imperfect mixing conditions.

in Table 5, which are also obtained from the available literature (Brandrup and Immergut, 1989).

MWD of the mixing model

Since the shape of the MWD may have a significant impact on the final polymer properties, understanding the influence of mixing on the full MWD is important. If the instantaneous MWD in each mixing zone is represented by some known distribution functions such as log-normal distribution, the overall MWD from the whole reactor is the weighted summation of the instantaneous MWD in each zone. The parameters of the instantaneous distribution function can be calculated from the instantaneous polymer properties, which only depend upon the rate of change of the polymer moments and are independent of the inflow conditions.

$$\text{Inst}\,DP_n = \frac{R\lambda_{1,0}}{R\lambda_{0,0}} \tag{26}$$

$$\text{Inst}\,Z_p = \frac{R\lambda_{2,0}R\lambda_{0,0}}{(R\lambda_{1,0})^2}. \tag{27}$$

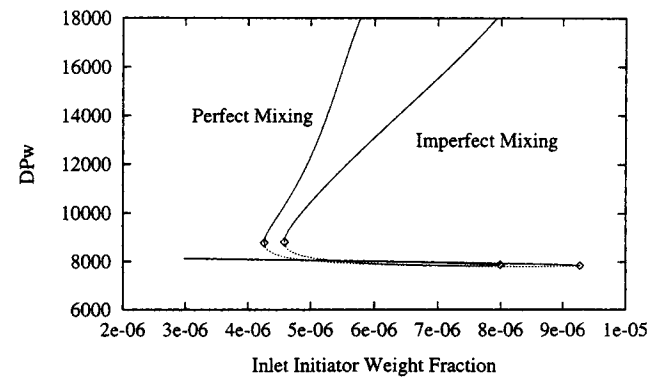

Figure 8. Continuation diagram of weight average chain length.

Steady-state weight average chain length (DP_w) is shown as a function of the inlet initiator concentration under both perfect and imperfect mixing conditions.

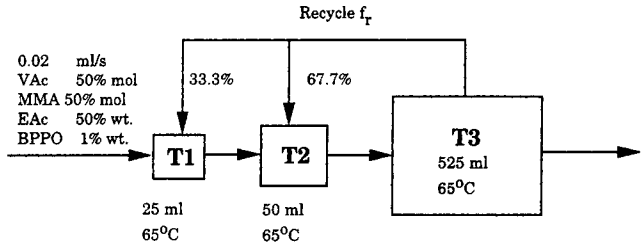

Figure 9. Mixing model for vinyl acetate/MMA copolymerization; the model is the same as the one used for the LDPE autoclave.

The MWD of each mixing zone and the overall MWD of the imperfectly mixed reactor are shown in Figure 10. The MWD curves shown here are the equivalent GPC curves. The instantaneous MWD in each mixing zone is different because of the different local environments (e.g., initiator concentrations). Because the initiator decomposes extremely fast, small injection zones have higher initiator concentrations and subsequently produce shorter polymer chains than the bulk of the reactor. As a result, although the MWD in each zone is symmetric log-normal distribution, the overall MWD is a distorted distribution with a shoulder in the high molecular-weight region.

Linear and nonlinear polymerization

In linear polymerization systems, there is no significant branching or transfer to polymer reaction and the chains produced are linear. However, in nonlinear polymerization, significant branching exists and the polymers produced are highly branched. Depending on whether the polymerization is linear or nonlinear, the influences of mixing on the MWD are different.

Figure 11 shows the polydispersity (Z_p) as a function of the reactor residence time for the vinyl acetate (VAc)/MMA

Table 5. Kinetic Rate Constants of VAc/MMA Copolymerization

Monomer	Reaction	k_0 (L/mol·s)	E_a (cal/mol)
Vinyl acetate	Initiation k_d (BPPO)	1.763×10^{12}	21,750
	Propagation k_p	3.2×10^{7}	6,300
	Termination k_{td}	3.70×10^{9}	3,200
	Transfer to polymer k_{trp}	1.088×10^{4}	6,300
	Transfer to solvent k_{trs}	3.4244×10^{3}	6,300
	Transfer to monomer k_{trm}	7.616×10^{3}	6,300
	Transfer to CBr_4 k_{tra}	1.248×10^{9}	6,300
Methyl methacrylate	Propagation k_p	4.92×10^{5}	4,353
	Termination $k_{tc}+k_{td}$	9.8×10^{7}	701
	Termination k_{td}/k_{tc}	2.483×10^{3}	4,073
	Transfer to solvent k_{trs}	4.92	4,353
	Transfer to monomer k_{trm}	4.39×10^{2}	4,640
	Transfer to CBr_4 k_{tra}	1.328×10^{5}	6,300
Reactivity ratios	Propagation	$r_1 = 0.03$	$r_2 = 26.0$

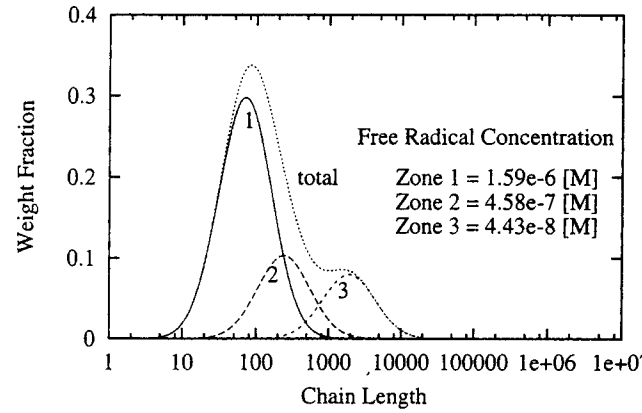

Figure 10. MWD of VAc/MMA copolymerization in an imperfectly mixed reactor.

The instantaneous MWD in each zone is assumed to be a lognormal distribution. Simulation parameters: $f_r = 0.5$, $f_1 = 0.33$, residence time = 30,000 s, inlet monomer composition = 0.5.

copolymerization and as a function of the inlet initiator concentration for the LDPE autoclave. For the VAc/MMA system, a perfectly mixed reactor yields a low Z_p of 2 for the entire residence time; while for an imperfectly mixed reactor, Z_p increases linearly with the residence time due to the concentration nonuniformity inside the reactor. The exit polymer is a blend of polymers produced in the different zones under different conditions and thus have a broader MWD than the polymer produced in each zone.

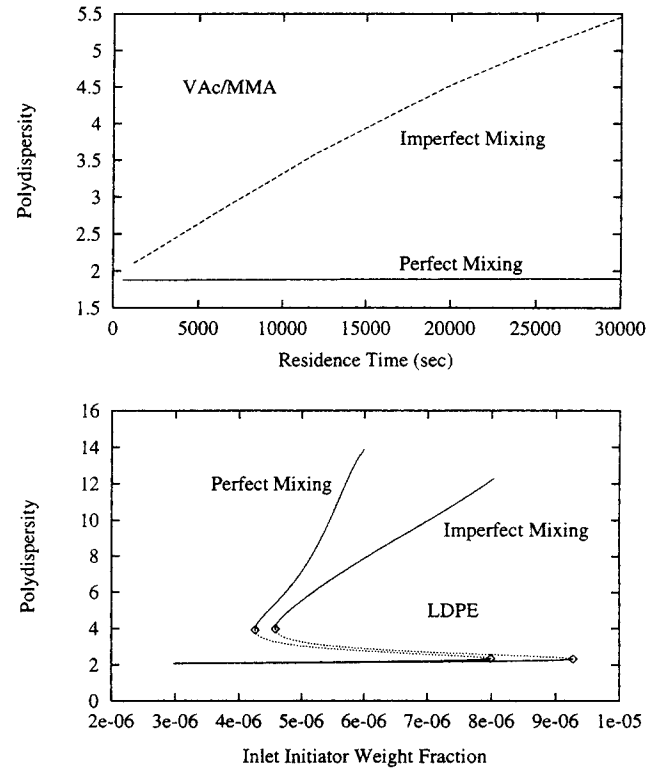

Figure 11. Continuation diagram of polydispersity.

Steady-state polydispersities are shown for the VAc/MMA solution copolymerization and the LDPE autoclave.

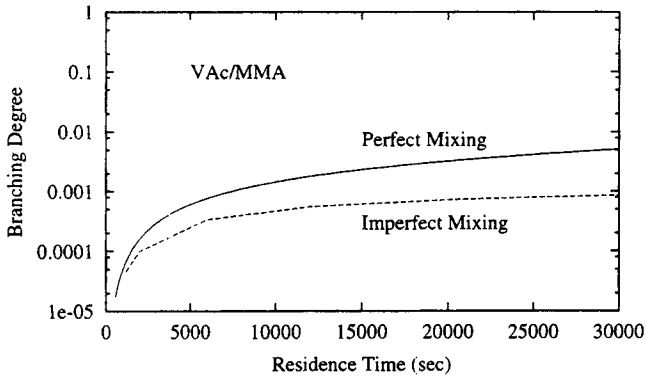

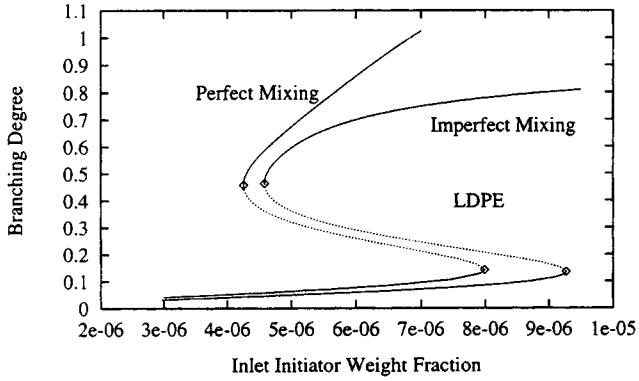

Figure 12. Continuation diagram of branching degree.

Steady-state branching degrees are shown for the VAc/MMA solution copolymerization and the LDPE autoclave.

By contrast, in an LDPE autoclave, polymers with higher polydispersity are produced under perfect mixing, which is different from the common belief that imperfect mixing always causes higher polydispersity because of the nonuniformity of species concentrations.

The differences in polydispersity between the LDPE and the VAc/MMA systems are due to different kinetic mechanisms, specifically the branching reaction for LDPE. Figure 12 shows the branching degree for both systems. Although vinyl acetate has relatively high transfer to polymer reactions, long-chain branching is not significant in the VAc/MMA system studied here (less than 0.001 branch per chain) because of high solvent concentrations and the presence of a nonbranching comonomer MMA. However, the LDPE polymerization has strong branching reactions and the polymers produced are highly branched (0.4–0.8 branch per chain). Thus, while the nonuniformity in small molecules such as initiator and monomers dominates the MWD in the VAc/MMA system, the fact that high radical concentrations are in regions of low dead polymer concentration and vice versa leading to reduced branching dominates the MWD in the LDPE system. Hence, mixing effects dominate in the VAc/MMA system, while kinetic effects dominate in the LDPE system. Considering both kinetic and mixing effects is important in understanding how the mixing will influence the MWD, because branching effects can sometimes overcome the effects of linear chain nonuniformity caused by imperfect mixing.

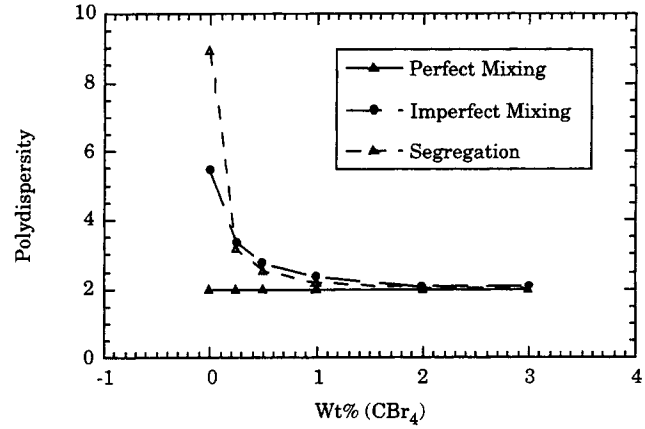

Figure 13. Effects of chain transfer agent on polydispersity; VAc/MMA copolymerization with mixing parameters as: $f_r = 0.86$, $f_1 = 0.333$.

Chain transfer agents

In linear polymerization systems we have seen that poor mixing causes a broader MWD. If low polydispersity is desired under imperfect mixing conditions, we can take advantage of the kinetics to reduce the mixing effects. Since high polydispersity under imperfect mixing is caused by significant heterogeneity in initiator concentration, if the dominant chain termination steps are changed to reactions other than the usual radical termination, mixing effects on the MWD can be reduced. For example, using a chain transfer agent (CTA) will change the dominant termination mechanism to chain transfer to the transfer agent.

Figure 13 shows the effects of a chain transfer agent (CBr_4) on polydispersity in VAc/MMA copolymerization. The polydispersity decreases dramatically with increasing CTA concentration in an imperfectly mixed reactor. When the inlet CBr_4 concentration is greater than 2%, both perfect and imperfect mixing yield similar low polydispersity. However, there is a well-known trade-off between polydispersity and chain length, shown in Figure 14. Thus there must be an optimal combination of initiator and CTA concentrations to achieve the desired polydispersity and chain length with acceptable production rate.

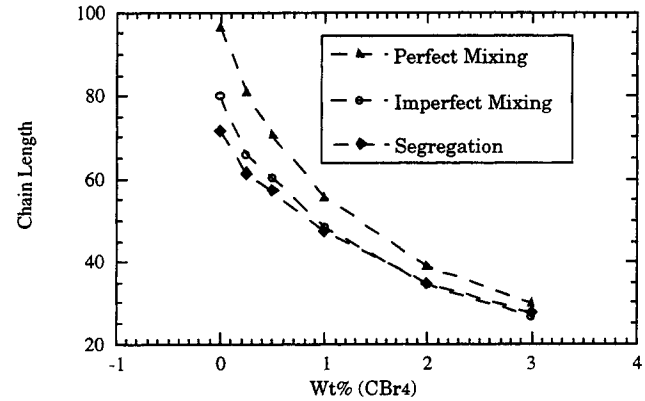

Figure 14. Effects of chain transfer agent on chain length; VAc/MMA copolymerization with mixing parameters as: $f_r = 0.86$; $f_1 = 0.33$.

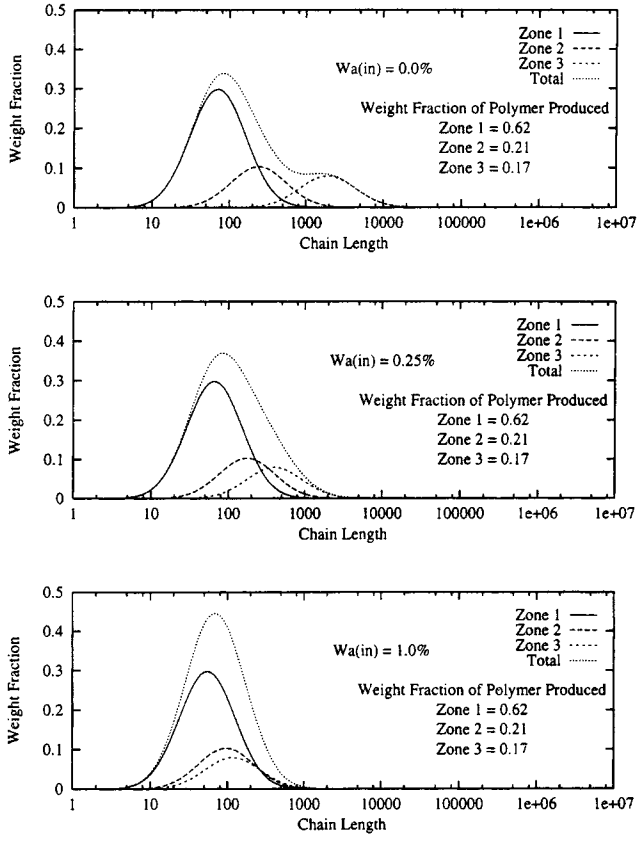

Figure 15. Influence of chain transfer agent on the MWD.

The influence of CBr_4 feed concentration, Wa(in), on the MWD in the VAc/MMA copolymerization. Instantaneous MWD in each zone is assumed to be a lognormal distribution. Simulation parameters: $f_r = 0.5$, $f_1 = 0.33$.

Figure 15 shows the influence of CTA on the instantaneous MWDs in different regions and on the overall MWD. Without CTA the instantaneous MWDs in the different regions are quite different and the overall MWD has a tail in the high molecular-weight region. However, as the CTA concentration increases, chain transfer becomes the dominant chain-termination mechanism, and the CTA concentrations are relatively uniform inside the reactor. The MWD in each zone then becomes more uniform and moves toward the lower molecular-weight region. The overall MWD becomes narrower, but shifts toward lower molecular weight.

Mixing and Copolymer Properties

Copolymer composition and chain sequence length are important in copolymerization because they affect the final polymer properties. Depending on reactivity ratios and monomer compositions, the copolymer properties can be affected by mixing. Figure 16 shows copolymer composition (F_{P_1}) as a function of unreacted monomer composition (F_{M_1}) for the styrene/MMA and VAc/MMA systems, where F_{P_1} and F_{M_1} refer to the first monomer in the copolymerization pair (styrene and VAc). For the styrene/MMA system, the monomer reactivity ratios are similar ($r_1 = 0.46$, $r_2 = 0.49$) and F_{P_1} is close to F_{M_1} with an azeotropic point around $F_{M_1} = 0.5$. However, for the VAc/MMA system, the monomers have

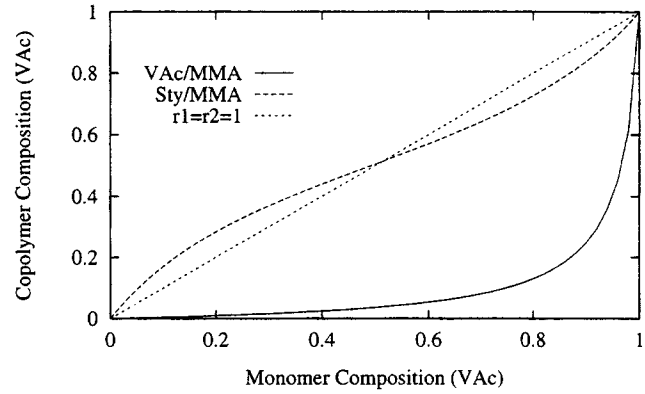

Figure 16. Copolymer composition diagram.

Copolymer compositions (F_{P_1}) as functions of monomer composition (F_{M_1}) for the styrene/MMA and VAc/MMA systems.

significantly different reactivity ratios ($r_1 = 0.03$, $r_2 = 26$) and F_{P_1} is significantly different from F_{M_1}. Hence, for the styrene/MMA system the monomer composition change will not have a significant impact on the copolymer composition. However, for the VAc/MMA system at F_{M_1} around 0.9, any small change in the monomer composition will dramatically change the copolymer composition.

Imperfect mixing creates heterogeneity in monomer compositions and affects copolymer composition accordingly. Figure 17 shows the influence of mixing on the copolymer composition (F_{P_1}) at two different monomer feed compositions (F_{fM_1}, 0.5 and 0.9) for both styrene/MMA and VAc/MMA systems. Note that the exit monomer composition (F_{M_1}) is different from the feed (F_{fM_1}) and has a higher concentration of less-reactive monomer (e.g., VAc). Because of different reaction environments, the exit monomer composition is also different for the perfect and imperfect mixing cases.

For the styrene/MMA system, F_{P_1} (styrene) is almost independent of the mixing conditions at 0.5 monomer feed composition F_{fM_1} and only slightly affected when F_{fM_1} is changed to 0.9. However, for the VAc/MMA system, F_{P_1} (VAc) is strongly affected by mixing for F_{fM_1} of 0.5, and the influence is even more pronounced if F_{fM_1} is 0.9.

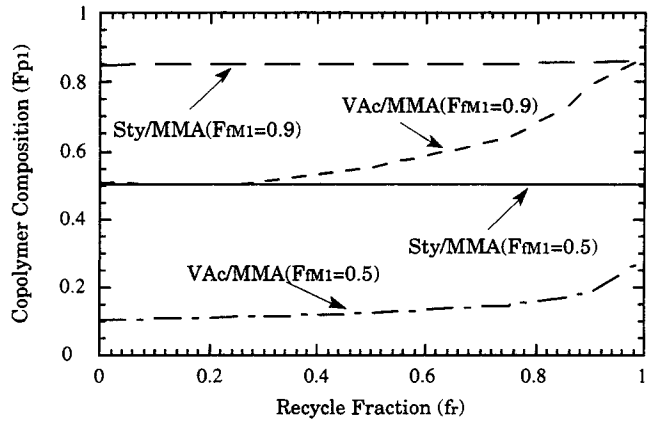

Figure 17. Effects of mixing on copolymer composition.

Steady-state copolymer composition as a function of mixing intensity at two different monomer feed compositions (0.5 and 0.9) for styrene/MMA and VAc/MMA systems.

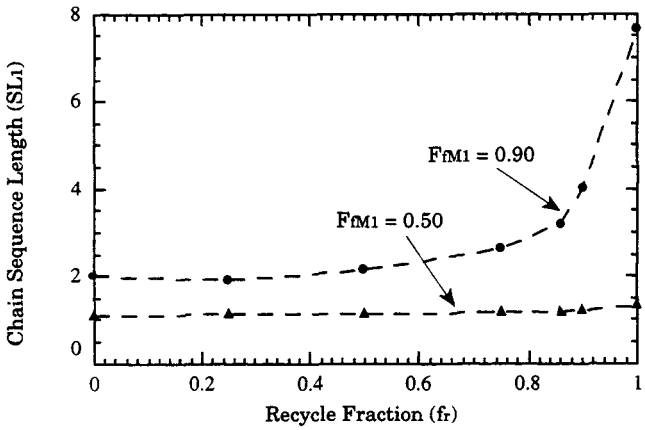

Figure 18. Effects of mixing on chain sequence length.

Steady-state chain sequence length as a function of mixing intensity at two different monomer feed compositions (0.5 and 0.9) for VAc/MMA system.

Figure 18 shows the influence of mixing on the average chain sequence length (SL_1) in the VAc/MMA system. The chain sequence length is also strongly affected by the mixing due to the difference in the monomer reactivity ratios and the heterogeneity in monomer composition. The influence of mixing is more important when F_{fM_1} is 0.9. By contrast, the chain sequence length for the styrene/MMA system is hardly affected by imperfect mixing (Zhang, 1996). Hence, mixing has a larger impact when the combined effects of reactivity ratio and monomer composition cause the copolymer composition to be very sensitive to monomer composition.

Conclusion

A compartmental mixing model is used to study imperfect mixing and its effects on polymer properties. Three polymerization systems are studied because of their industrial importance and unique kinetics: tyrene homopolymerization, high-pressure ethylene homopolymerization, and VAc/MMA solution copolymerization. The full MWD under imperfect mixing conditions is constructed from the leading moments based on predefined distributions. Continuation analysis indicates that mixing affects reactor steady states, stability, and polymer properties. The results suggest that both kinetic and mixing effects have to be considered in understanding how imperfect mixing affects the polymer MWD.

In linear polymerization systems, imperfect mixing broadens the MWD. However, in nonlinear polymerization systems with significant branching, depending on the reaction conditions, imperfect mixing can broaden or narrow the MWD. Branching and chain transfer reactions are among the important mechanisms in determining the mixing effects on polymer properties. By changing the dominant chain-termination mechanism to chain transfer to transfer agents, the influence of imperfect mixing on the MWD can be reduced. When copolymer composition is sensitive to monomer composition, mixing also significantly affects copolymer properties.

Acknowledgment

The authors are indebted to the National Science Foundation and the Industrial Sponsors of the University of Wisconsin Polymerization Reaction Engineering Laboratory (UWPREL) for the financial support. We are also grateful to Dr. Nolan K. Read of DuPont for discussions and to Dr. Zhengfang Xu for help during the revision.

Notation

Ak = apparent rate constants, $mol \cdot L^{-1} \cdot s^{-1}$
c_p = total specific heat, $cal \cdot g^{-1} \cdot °C^{-1}$
C_I = initiator concentration, $mol \cdot L^{-1}$
C_{M_i} = concentration of monomer i, $mol \cdot L^{-1}$
C_S = solvent concentration, $mol \cdot L^{-1}$
C_A = chain transfer agent concentration, $mol \cdot L^{-1}$
$[D_n]$ = concentration of terminal double bond, $mol \cdot L^{-1}$
DTBP = ditert butyl peroxide
E_a = activation energy, $cal \cdot g^{-1}$
f = initiator decomposition efficiency
k_b = backbiting rate constant, s^{-1}
k_d = initiator decomposition rate constant, s^{-1}
k_p = propagation rate constant, $L \cdot mol^{-1} \cdot s^{-1}$
k_{tc} = termination by combination rate constant, $L \cdot mol^{-1} \cdot s^{-1}$
k_{td} = termination by disproportionation rate constant, $L \cdot mol^{-1} \cdot s^{-1}$
k_{tra} = chain transfer to agent rate constant, $L \cdot mol^{-1} \cdot s^{-1}$
k_{trp} = transfer to polymer rate constant, $L \cdot mol^{-1} \cdot s^{-1}$
k_{trs} = chain transfer to solvent rate constant, $L \cdot mol^{-1} \cdot s^{-1}$
Mw_i = molecular weight of component i, $g \cdot mol^{-1}$
P = reactor pressure, atm
R_i = species i kinetic rate of change, $mol \cdot L^{-1} \cdot s^{-1}$
r_{ij} = reactivity ratio
T = temperature, °C
V = volume of reaction mixture, cm^3
W_S = solvent weight fraction in the reaction mixture
X_p = fractional conversion of monomer to polymer
$(\Delta H)_r$ = enthalpy of reaction r, $cal \cdot mol^{-1}$
ρ = total density, $g \cdot cm^{-3}$

Literature Cited

Arriola, D. J., "Modeling of Addition Polymerization Systems," PhD Thesis, Univ. of Wisconsin-Madison (1989).

Atiqullah, M., and E. B. Nauman, "A Model and Measurement Technique for Micromixing in Copolymerization Reactors," *Chem. Eng. Sci.*, **45**(5), 1267 (1990).

Baade, W., H. U. Moritz, and K. H. Reichert, "Kinetics of High Conversion Polymerization of Vinyl Acetate. Effects of Mixing and Reactor Type on Polymer Properties," *J. Appl. Poly. Sci.*, **27**, 2249 (1982).

Baldyga, J., and J. R. Bourne, "A Fluid Mechanical Approach to Turbulent Mixing and Chemical Reaction. Part II: Micromixing in the Light of Turbulence Theory," *Chem. Eng. Commun.*, **28**, 243 (1984).

Blavier, L., and J. Villermaux, "Free Radical Polymerization Engineering: II. Modeling of Homogeneous Polymerization of Styrene in a Batch Reactor, Influence of Initiator," *Chem. Eng. Sci.*, **39**, 101 (1984).

Brandrup, J., and E. H. Immergut, *Polymer Handbook*, 3rd ed., Wiley, New York (1989).

Call, M., and R. Kadlec, "Estimation of Micromixing Parameters from Tracer Concentration Fluctuation Measurement," *Chem. Eng. Sci.*, **44**, 1377 (1989).

Chan, W.-M., P. E. Gloor, and A. E. Hamielec, "A Kinetic Model for Olefin Polymerization in High Pressure Autoclave Reactors," *AIChE J.*, **39**, 111 (1993).

Chen, C. H., J. G. Vermeychuk, J. A. Howell, and P. Ehrlich, "Computer Model for Tubular High-Pressure Polyethylene Reactor," *AIChE J.*, **22**(3), 463 (1976).

Curl, R. L., "Dispersed Phase Mixing: I. Theory and Effects in Simple Reactors," *AIChE J.*, **9**, 175 (1963).

Fields, S. D., and J. M. Ottino, "Effect of Striation Thickness Distribution on the Course of an Unpremixed Polymerization," *Chem. Eng. Sci.*, **42**, 459 (1987).

Fox, R. O., and J. Villermaux, "Unsteady State IEM Model: Numerical Simulation and Multiple-Scale Perturbation Analysis Near Perfect-Micromixing Limit," *Chem. Eng. Sci.*, **45**, 373 (1990).

Goto, S., and M. Matsubara, "A Generalized Two-Environment Model for Micromixing in a Continuous Flow Reactor: I. Construction of the Model," *Chem. Eng. Sci.*, **30**, 61 (1975).
Goto, S., K. Yamamoto, S. Furui, and M. Sugomoto, "Computer Model for Commercial High Pressure Polyethylene Reactor Based on Elementary Reaction Steps Obtained Experimentally," *J. Appl. Poly. Sci.*, **36**, 21 (1981).
Hamielec, A. E., and J. F. MacGregor, "Modeling Copolymerization —Control of Composition, Chain Microstructure, Molecular Weight Distribution, Long Chain Branching and Crosslinking," *Polymer Reaction Engineering*, K. H. Reichert and W. Geiseler, eds., Hansher, Berlin, p. 21 (1983).
Harada, M., K. Tanaka, W. Eguchi, and S. Nagata, "The Effect of Micro-Mixing on the Homogeneous Polymerization of Styrene in a Continuous Flow Reactor," *J. Chem. Eng. Japan*, **1**, 148 (1968).
Hatate, Y., T. Ikeura, M. Shinonome, and K. Kondo, "Suspension Polymerization of Styrene under Ultrasonic Irradiation," *J. Chem. Eng. Japan*, **14**, 38 (1981).
Hyanek, I., J. Zacca, F. Teymour, and W. H. Ray, "Dynamics and Stability of Polymerization Process Flow Sheets," *Ind. Eng. Chem. Res.*, **34**, 3872 (1995).
Kalbfleisch, B., and F. Teymour, "Segregation Effects on the Dynamics of Continuous Reactors for Nonlinear Polymerization," AIChE Meeting, Miami (1995).
Kalfas, G., and W. H. Ray, "Modeling and Experimental Studies of Aqueous Suspension Polymerization Processes. I. Modeling and Simulation," *Ind. Eng. Chem. Res.*, **32**, 1822 (1993).
Kattan, A., and R. J. Adler, "A Conceptual Framework for Mixing in Continuous Chemical Reactors," *Chem. Eng. Sci.*, **27**, 1013 (1972).
Kuo, J. F., C. Y. Chen, C. W. Chen, and T. C. Pan, "The Apparent Rate Constant Model for Kinetics of Radical Chain Copolymerization: Chemical-controlled Process," *Poly. Eng. Sci.*, **24**, 22 (1984).
Marini, L., and C. Georgakis, "Low Density Polyethylene Vessel Reactors," *AIChE J.*, **30**, 401 (1984a).
Marini, L., and C. Georgakis, "The Effect of Imperfect Mixing on Polymer Quality in Low Density Polyethylene Vessel Reactor," *Chem. Eng. Commun.*, **30**, 361 (1984b).
Mecklenburgh, J. C., "The Influence of Mixing on the Distribution of Copolymerization Composition," *Can. J. Chem. Eng.*, **48**, 279 (1970).
Mehta, R. V., and J. M. Tarbell, "A Four-Environmental Model of Chemical Reaction: Model Development," *AIChE J.*, **29**, 320 (1983).
Nauman, E. B., "The Droplet Diffusion Model for Micromixing," *Chem. Eng. Sci.*, **30**, 1135 (1975).
Ochs, S., P. Rosendorf, I. Hyanek, X. Zhang, and W. H. Ray, "Dynamic Flowsheet Modelling of Polymerization Process Using POLYRED," *Comput. Chem. Eng.*, **20**, 657 (1996).
O'Driscoll, K. F., and R. Knorr, "Multicomponent Polymerization: II. The Effect of Mixing on Copolymerization in Continuous Stirred Tank Reactors," *Macromolecules*, **2**, 507 (1969).
Ray, W. H., "On the Mathematical Modeling of Polymerization Reactors," *J. Macrmol. Sci.-Rev. Macromol. Chem. Phys.*, **C8**, 1 (1972).
Read, N. K., S. X. Zhang, and W. H. Ray, "Simulation of an Industrial Scale Low Density Polyethylene Autoclave Reactor using Computation Fluid Dynamics," *AIChE J.*, **3**, 104 (1997).
Ritchie, B. W., and A. H. Tobgy, "General Population Balance Modelling of Unpremixed Feedstream Chemical Reactors: A Review," *Chem. Eng. Commun.*, **2**, 249 (1978).
Sahm, P., "Effects de Microemlange sur la Polymerisation Radiclaire du Styrene en Reacteur Agite Continu," PhD Thesis, Institut National Polytechnique de Lorraine, Nancy (1978).
Smit, L., "The Use of Micromixing Calculations in LDPE-Reactor-modelling," *Proc. Workshop on Polymer Reaction Engineering*, K. H. Reichert and H. U. Moritz, eds., DECHEMA, p. 77 (1992).
Spielman, L. A., and O. Levenspiel, "A Monte Carlo Treatment for Reacting and Coalescing Dispersed Phase Systems," *Chem. Eng. Sci.*, **20**, 247 (1964).
Tadmor, Z., and J. A. Biesenberger, "Influence of Segregation on Molecular Weight Distribution in Continuous Linear Polymerizations," *Ind. Eng. Chem. Fund.*, **5**, 336 (1966).
Torvik, R., A. R. Gravdahl, G. R. Fredriksen, O. Meon, and J. Laurell, "Design of HPPE Stirred Autoclaves using 3D Computational Fluid Dynamics," *Proc. Workshop on Polymer Reaction Engineering*, K. H. Reichert and H. U. Moritz, eds., DECHEMA, p. 401 (1995).
Tosun, G., "A Mathematical Model of Mixing and Polymerization in a Semibatch Stirred-Tank Reactor," *AIChE J.*, **38**, 425 (1992).
Tsai, K., and R. O. Fox, "CFD/PDF Simulation of LDPE Polymerization in a Tubular Reactor," AIChE Meeting, Miami (1995).
Van der Molen, T. J., and A. Keonen, "Effect of Process Conditions on Light-Off Temperature and Consumption of 16 Initiators, as Determined from High Pressure Radical Polymerization of Ethylene," Colloq. on Chemical Reactions Engineering, Novara, Italy (1981).
Villermaux, J., "A Simple Model for Partial Segregation in a Semi-Batch Reactor," AIChE Meeting, San Francisco (1989).
Villermaux, J., "Mixing Effects on Complex Chemical Reactions in a Stirred Tank," *Rev. Chem. Eng.*, **7**(1), 51 (1991).
Villermaux, J., and A. Zoulalian, "Etat de melange du fluid dans un reacteur continu-a props d'un modele de Weinstein er Adler," *Chem. Eng. Sci.*, **24**, 1513 (1969).
Weinstein, H., and R. J. Adler, "Micromixing Effects in Continuous Chemical Reactors," *Chem. Eng. Sci.*, **22**, 65 (1967).
Zacca, J., X. Zhang, and H. W. Ray, "Reactor Runaway Phenomena in Polymerization Processes," *Proc. Int. Symp. on Runaway Reaction and Pressure Relief Design*, H. Fisher, ed., AIChE, New York (1995).
Zhang, S. X., "Modelling and Experimental Studies of Free Radical Polymerization Reactors," PhD Thesis, Univ. of Wisconsin-Madison (1996).
Zhang, S. X., N. K. Read, and W. H. Ray, "Runaway Phenomena in Low-density Polyethylene Autoclave Reactors," *AIChE J.*, **42**, 2911 (1996).

Appendix

Live polymer moments

The live polymer chain-length distribution moments in a CSTR are

$$\frac{d\mu_{0,0}}{dt} = \frac{Q^{\text{in}}}{V}\mu_{0,0}^{\text{in}} - \frac{Q}{V}\mu_{0,0} - \frac{1}{V}\frac{dV}{dt}\mu_{0,0} + \sum_j 2f_j k_{d_j} C_{I_j} + gk_i C_M{}^{b_i} h\gamma^{c_i} - (k_{tc} + k_{td})\mu_{0,0}^2 - (k_{tx}C_X + k_{tsp})\mu_{0,0} \quad \text{(A1)}$$

$$\frac{d\mu_{1,0}}{dt} = \frac{Q^{\text{in}}}{V}\mu_{1,0}^{\text{in}} - \frac{Q}{V}\mu_{1,0} - \frac{1}{V}\frac{dV}{dt}\mu_{1,0} + k_p C_M \mu_{0,0} - k_{prv}(\mu_{0,0} - P_1) - (k_{tc} + k_{td})\mu_{1,0}\mu_{0,0} - (k_{trm}C_M + k_{trs}C_S + k_{tra}C_A + k_{trsp})\mu_{1,0} - (k_{tx}C_X + k_{tsp})\mu_{1,0} - P_b k_{\beta 1}\mu_{1,0} + k_{trp}(\lambda_{2,0}\mu_{0,0} - \lambda_{1,0}\mu_{1,0}) - \frac{1}{2}P_{trp}k_{\beta 2}(\lambda_{2,0} - \lambda_{1,0})\mu_{0,0} + k_{TDB}[D_n]\lambda_{1,0}\mu_{0,0} \quad \text{(A2)}$$

$$\frac{d\mu_{2,0}}{dt} = \frac{Q^{\text{in}}}{V}\mu_{2,0}^{\text{in}} - \frac{Q}{V}\mu_{2,0} - \frac{1}{V}\frac{dV}{dt}\mu_{2,0} + k_p C_M(\mu_{0,0} + 2\mu_{1,0}) - k_{prv}(2\mu_{1,0} - \mu_{0,0} - P_1) - (k_{tc}+k_{td})\mu_{2,0}\mu_{0,0} - (k_{trm}C_M + k_{trs}C_S + k_{tra}C_A + k_{trsp})\mu_{2,0} - (k_{tx}C_X + k_{tsp})\mu_{2,0} - P_b k_{\beta 1}\mu_{2,0} + k_{trp}(\lambda_{3,0}\mu_{0,0} - \lambda_{1,0}\mu_{2,0}) - P_{trp}k_{\beta 2}\left(\frac{2}{3}\lambda_{3,0} - \frac{\lambda_{2,0}}{2} - \frac{\lambda_{1,0}}{6}\right)\mu_{0,0} + k_{TDB}[D_n](2\lambda_{1,0}\mu_{0,0} + \lambda_{2,0}\mu_{0,0}). \quad \text{(A3)}$$

The live polymer branching distribution moment in a CSTR is

$$\frac{d\mu_{0,1}}{dt} = \frac{Q^{in}}{V}\mu_{0,1}^{in} - \frac{Q}{V}\mu_{0,1} - \frac{1}{V}\frac{dV}{dt}\mu_{0,1} - (k_{tc}+k_{td})\mu_{0,1}\mu_{0,0} - (k_{trm}C_M + k_{trs}C_S + k_{tra}C_A + k_{trsp})\mu_{0,1} - (k_{tx}C_X + k_{tsp})\mu_{0,1} - P_b k_{\beta 1}\mu_{0,1} + k_{trp}(\lambda_{1,0}\mu_{0,0} + \lambda_{1,1}\mu_{0,0} - \lambda_{1,0}\mu_{0,1}) - P_{trp}k_{\beta 2}\left(\lambda_{1,0} + \frac{\lambda_{1,1}}{2}\right)\mu_{0,0} + k_{TDB}[D_n](\lambda_{0,0} + \lambda_{0,1})\mu_{0,0}. \quad \text{(A4)}$$

Under the QSSA, the differential equations for the live polymer moments become algebraic equations, which can be solved explicitly for the live polymer moments $\mu_{0,0}$, $\mu_{1,0}$, and $\mu_{0,1}$.

Bulk polymer moments

The bulk polymer chain length distribution moments in a CSTR are

$$\frac{d\lambda_{0,0}}{dt} = \frac{Q^{in}}{V}\lambda_{0,0}^{in} - \frac{Q}{V}\lambda_{0,0} - \frac{1}{V}\frac{dV}{dt}\lambda_{0,0} + \sum_j 2f_j k_{d_j} C_{I_j} + gk_i C_M^{b_i} h\gamma^{c_i} + (k_{trm}C_M + k_{trs}C_S + k_{tra}C_A + k_{trsp})\mu_{1,0} - \frac{k_{tc}}{2}\mu_{0,0}^2 + P_b k_{\beta 1}\mu_{1,0} + P_{trp}k_{\beta 2}(\lambda_{2,0} - \lambda_{1,0})\mu_{0,0} - k_{TDB}[D_n]\lambda_{0,0}\mu_{0,0} \quad \text{(A5)}$$

$$\frac{d\lambda_{1,0}}{dt} = \frac{Q^{in}}{V}\lambda_{1,0}^{in} - \frac{Q}{V}\lambda_{1,0} - \frac{1}{V}\frac{dV}{dt}\lambda_{1,0} + k_p C_M \mu_{0,0} - k_{prv}(\mu_{0,0} - P_1) \quad \text{(A6)}$$

$$\frac{d\lambda_{2,0}}{dt} = \frac{Q^{in}}{V}\lambda_{2,0}^{in} - \frac{Q}{V}\lambda_{2,0} - \frac{1}{V}\frac{dV}{dt}\lambda_{2,0} + 2(k_p C_M - k_{prv})\mu_{1,0} + k_{tc}\mu_{1,0}^2 - P_{trp}k_{\beta 2}(\lambda_{3,0} - \lambda_{1,0})\mu_{0,0} + 2k_{TDB}[D_n]\lambda_{1,0}\mu_{1,0} \quad \text{(A7)}$$

$$\frac{d\lambda_{3,0}}{dt} = \frac{Q^{in}}{V}\lambda_{3,0}^{in} - \frac{Q}{V}\lambda_{3,0} - \frac{1}{V}\frac{dV}{dt}\lambda_{3,0} + 3k_p C_M(\mu_{2,0} + \mu_{1,0}) - 3k_{prv}(\mu_{2,0} - \mu_{1,0}) + 3k_{tc}\mu_{2,0}\mu_{1,0} - \frac{P_{trp}k_{\beta 2}\mu_{0,0}}{2}(\lambda_{4,0} - \lambda_{2,0}) + 3k_{TDB}[D_n](\lambda_{1,0}\mu_{2,0} + \lambda_{2,0}\mu_{1,0}). \quad \text{(A8)}$$

The bulk polymer branching distribution moments in a CSTR are

$$\frac{d\lambda_{0,1}}{dt} = \frac{Q^{in}}{V}\lambda_{0,1}^{in} - \frac{Q}{V}\lambda_{0,1} - \frac{1}{V}\frac{dV}{dt}\lambda_{0,1} + k_{trp}\lambda_{1,0}\mu_{0,0} - P_{trp}k_{\beta 2}\lambda_{1,0}\mu_{0,0} + k_{TDB}[D_n]\lambda_{0,0}\mu_{0,0} \quad \text{(A9)}$$

$$\frac{d\lambda_{1,1}}{dt} = \frac{Q^{in}}{V}\lambda_{1,1}^{in} - \frac{Q}{V}\lambda_{1,1} - \frac{1}{V}\frac{dV}{dt}\lambda_{1,1} + k_p C_M \mu_{0,1} - k_{prv}\mu_{0,1} + k_{tc}\mu_{1,1}\mu_{0,1} + k_{trp}\lambda_{2,0}\mu_{0,0} - P_{trp}k_{\beta 2}\left(\lambda_{2,0} + \frac{\lambda_{2,1}}{2}\right)\mu_{0,0} + k_{TDB}[D_n][\lambda_{1,0}(\mu_{0,1} + \mu_{0,0}) + (\lambda_{1,0} + \lambda_{0,0})\mu_{0,0}]. \quad \text{(A10)}$$

Manuscript received Aug. 16, 1996, and revision received Jan. 9, 1997.